

Photospheric aluminium abundances of A-type main-sequence stars

Y. Takeda 

11-2 Enomachi, Naka-ku, Hiroshima-shi, 730-0851, Japan (E-mail:
ytakeda@js2.so-net.ne.jp)

Received: August 22, 2023; Accepted: October 16, 2023

Abstract. Although anomalous surface abundances are often observed in A-type main-sequence stars (known as chemically peculiar stars; e.g., metallic line stars or Am stars), our understanding about the behavior of aluminium is still insufficient. Actually, even whether Al is overabundant or underabundant in Am stars is not clarified. This is presumably because most of the previous studies employed the Al I 3944/3961 lines with the assumption of LTE, despite that a considerable non-LTE effect is expected in this resonance doublet. With an aim to shed light on this issue, extensive statistical-equilibrium calculations on Al I/Al II were carried out for a wide range of atmospheric parameters, based on which the non-LTE Al abundances were determined by applying the spectrum-fitting technique to the Al I 3944/3961 lines for 63 A-type dwarfs ($7000 \lesssim T_{\text{eff}} \lesssim 10000$ K) of comparatively lower rotational velocities ($v_e \sin i \lesssim 100 \text{ km s}^{-1}$). The following results were obtained. (1) The non-LTE corrections (Δ) are positive (reflecting the importance of overionization) and significantly large ($0.3 \lesssim \Delta \lesssim 1.0$ dex depending on T_{eff} ; generally $\Delta_{3944} < \Delta_{3961}$). (2) By applying these corrections (and indispensable inclusion of Balmer line wings as background opacity), consistent non-LTE abundances for both lines could be obtained, and the serious zero-point discrepancy (considerably negative [Al/H] for normal metallicity stars of $[\text{Fe}/\text{H}] \sim 0$) found in old studies has been settled. (3) Al abundances of A-type stars are almost in proportion to [Fe/H] (tending to be overabundant in Am stars) with an approximate relation of $[\text{Al}/\text{H}] \sim 1.2 [\text{Fe}/\text{H}]$, which is qualitatively consistent with the prediction of the diffusion theory (suggesting an Al excess in the photosphere of Am stars).

Key words: physical processes: diffusion – stars: abundances – stars: atmospheres – stars: chemically peculiar – stars: early-type

1. Introduction

An appreciable fraction of A-type stars ($7000 \lesssim T_{\text{eff}} \lesssim 10000$ K) on the upper main sequence are chemical peculiar (CP) stars. Among these, A-type metallic-line (Am) stars are commonly observed in comparatively slower rotators ($v_e \sin i \lesssim 100 \text{ km s}^{-1}$). While it is known that they show contrasting surface abundance anomalies between lighter and heavier elements (e.g., deficiency in

C, N, O, Ca, Sc; overabundances in Fe-group or s-process ones), abundance behaviors of those with intermediate atomic number ($10 < Z < 20$) are not necessarily well understood.

One of such elements for which abundances are poorly determined is aluminium (Al, $Z = 13$). This is not due to the lack of available lines, as strong resonance doublet lines of neutral aluminium at 3944 and 3961 Å are observable in the spectra of most A-type stars, although most Al atoms are in the once-ionized stage and only a tiny fraction remains neutral in stellar atmospheres of this T_{eff} range (Fig. 1). Actually, determinations of Al abundances in normal A-type and Am stars by using Al I 3944/3961 were reported already in the early work about a half century ago (e.g., Conti 1970; Smith 1971, 1973).

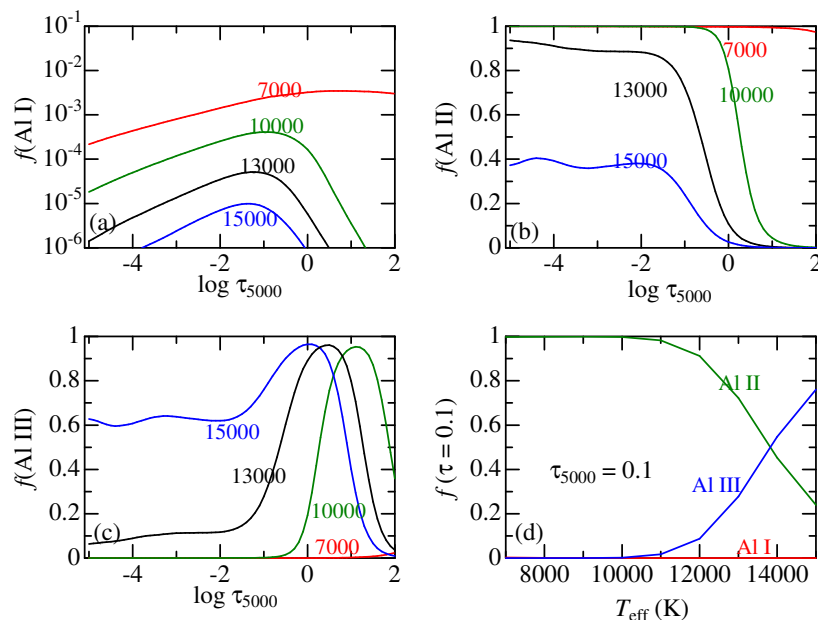


Figure 1. Number population fraction (f) of (a) neutral, (b) once-ionized, and (c) twice-ionized aluminium species relative to the total Al atoms [e.g., $f(\text{Al I}) \equiv N(\text{Al I})/N_{\text{total}}^{\text{Al}}$], plotted against the continuum optical depth at 5000 Å. Calculations were done for four $\log g = 4.0$ models of different T_{eff} (7000, 10000, 13000, and 15000 K) as indicated in each panel. The runs of f for these three stages at $\tau_{5000} = 0.1$ with T_{eff} are also depicted in panel (d). All these calculations were done in LTE (use of Saha’s equation).

Nevertheless, what was argued in those old studies was only qualitative that Al abundances in Am stars are comparatively higher than those in normal stars, while nothing could be said about the quantitative extent of Al anomalies with

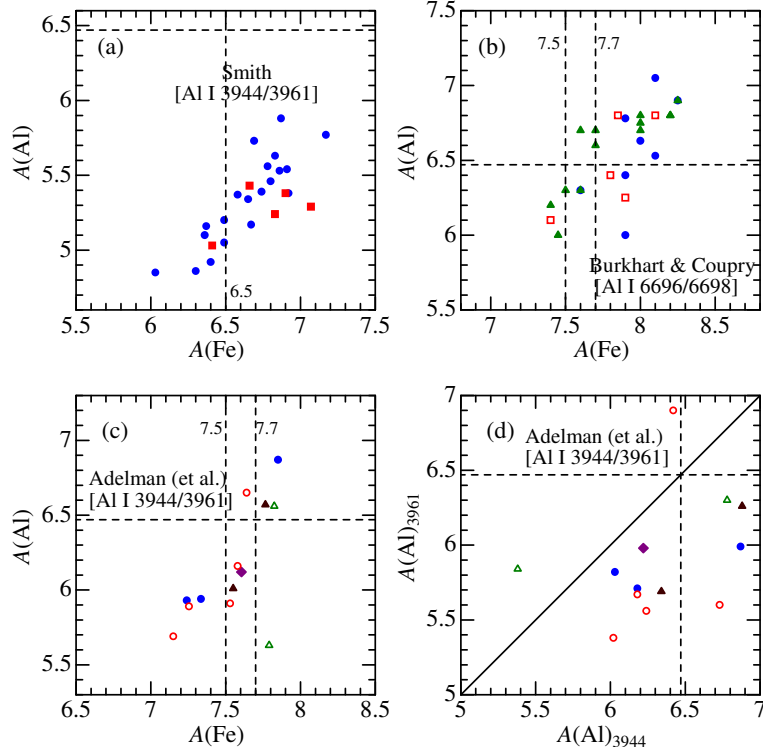


Figure 2. Panels (a)–(c) show the correlations of Al and Fe abundances published in the past literature. (a) Data of Smith (1971; circles) and Smith (1973; squares) based on Al I 3944/3961 lines. (b) Data of Burkhardt and Coupry (1989–circles; 1991–triangles, 2000–squares) based on Al I 6696/6698 lines. (c) Data of Adelman (1984–filled diamond), Adelman et al. (1984–open triangles), Adelman (1988–filled triangles), Adelman (1994–filled circles), and Adelman et al. (1997–open circles) based on Al I 3944/3961 lines. (d) A_{3944} vs. A_{3961} relation for Adelman et al.’s data in panel (c). In each panel, the locations of the solar Al abundance of $A_{\odot}(\text{Al}) = 6.47$ (adopted in this study) as well as of the solar Fe abundances believed at the time of the relevant papers (considerably revised over the past half century; cf. footnote 1) are indicated by dashed lines.

respect to the reference normal (solar) abundance¹ because absolute values of

¹ The solar photospheric abundance of aluminium $A_{\odot}(\text{Al})$ is considered to be well established (A is the logarithmic number abundance of the element relative to that of hydrogen with the usual normalization of $A = 12.00$ for H), for which quite similar values have been reported so far: 6.40 (Lambert, Warner 1968), 6.47 (Anders, Grevesse 1989), 6.45 (Asplund et al. 2009). In this paper, Anders and Grevesse’s $A_{\odot}(\text{Al})$ of 6.47 is adopted, as done in Kurucz’s (1993) ATLAS9/WIDTH9 program. In contrast, $A_{\odot}(\text{Fe})$ has experienced considerable updates from low-scale to high-scale over the past half century, mainly due to the large revision in the

the resulting Al abundances were far from reliable.

Since surface abundances of normal A-type stars of population I without chemical peculiarities should be more or less similar to the solar composition, $[\text{Al}/\text{H}] \sim 0$ is expected to hold for stars of $[\text{Fe}/\text{H}] \sim 0$.² However, according to Fig. 2a, where the Al abundances of A and Am stars derived by Smith (1971, 1973) from Al I 3944/3961 are plotted against the corresponding Fe abundances, the intercept of $[\text{Al}/\text{H}]$ at $[\text{Fe}/\text{H}] \sim 0$ is considerably subsolar ($\lesssim -1$ dex), which suggests that his $A(\text{Al})$ values were significantly underestimated. This zero-point discrepancy ($[\text{Al}/\text{H}] < 0$ at $[\text{Fe}/\text{H}] \sim 0$) is similarly observed in Adelman et al.'s results (cf. Fig. 2c), who also employed the Al I 3944/3961 lines for deriving the Al abundances of A-type stars. To make things more complicated, the abundances they derived from these two lines are systematically discordant from each other ($A_{3961} < A_{3944}$; cf. Fig. 2d). These are the problems involved with Al abundance determinations using these resonance lines.

Admittedly, this problem may be circumvented by invoking other Al lines. As a matter of fact, Burkhart and Coupry (1989, 1991, 2000) employed the high-excitation Al I 6696/6698 lines to derive Al abundances for late A-type and Am/Fm stars in the field and open clusters, and the resulting $[\text{Al}/\text{H}]$ values appear to favorably satisfy the requirement ($[\text{Al}/\text{H}] \sim 0$ at $[\text{Fe}/\text{H}] \sim 0$) mentioned above (cf. Fig. 2b). Unfortunately, these lines are so weak that are usable only for sharp-lined lower T_{eff} ($\lesssim 8000$ K) stars, which makes their applicability seriously limited. Accordingly, there is no other way than to avail of the strong Al I lines in the violet region if Al abundance behaviors of A-type stars in general are to be investigated.

Then, why are the Al abundances determined from 3944/3961 lines in the old studies unreliable and subject to appreciable errors (i.e., significantly underestimated)? The most likely reason is that they adopted the assumption of LTE in their analysis, because these Al I resonance lines are known to suffer a considerable non-LTE effect mainly caused by the overionization mechanism. Actually, Steenbock and Holweger (1992) carried out a statistical-equilibrium calculation in their analysis of Al I 3944 and 3961 lines of Vega and showed that rather large (positive) non-LTE corrections (+0.4 and +0.7 dex, respectively) should be applied. Since this correction acts in the direction of mitigating the underestimation, the problems involved in the Al abundances determined from 3944/3961 lines may be resolved by correctly taking into account the non-LTE effect.

However, ever since Steenbock and Holweger's (1992) non-LTE work confined to the specific case of Vega (a mildly metal-deficient A0V star), any investigation on the non-LTE effect of Al lines with regard to A-type stars in general has not been carried out to the author's knowledge, despite that not a few

transition probabilities of Fe lines (e.g., 6.5–7.0 \rightarrow 7.3–7.7 \rightarrow \sim 7.5; see Fig. 1 in Grevesse, Sauval 1999), though it is eventually settled around 7.50 at present (cf. Asplund et al. 2009).

² As usual, $[\text{X}/\text{H}]$ is the differential abundance of element X relative to the Sun; i.e., $[\text{X}/\text{H}] \equiv A_{\text{star}}(\text{X}) - A_{\odot}(\text{X})$.

non-LTE studies on Al I line formation for late-type stars (FGK type stars of $T_{\text{eff}} \lesssim 6500$ K; especially in the metal-poor regime for studying galactic chemical evolution) have already been published in the past quarter century (Baumüller, Gehren 1996, 1997; Mashonkina et al. 2008; Andrievsky et al. 2008; Nordlander, Lind 2017; Ezzeddine et al. 2018).

Motivated by this situation, the author decided to conduct extensive non-LTE calculations on Al I+Al II for a wide range of atmospheric parameters (covering main-sequence stars of mid-F through late-B types), and apply them to the analysis of Al I 3944/3961 lines for a sufficient number of A-type dwarfs by making use of the available high-dispersion spectra. The points intended to clarify in this investigation are as follows.

- How are the behaviors (e.g., characteristic trends, dependence upon atmospheric parameters) of the non-LTE effect for Al I 3944 and 3961 resonance doublet lines in upper main-sequence stars? Is there any significant difference between these two lines?
- To establish the Al abundance trends of A-type stars (Am and normal A stars) of various $[\text{Fe}/\text{H}]$ by applying the spectrum-fitting analysis to the 3944/3961 lines. Can the zero-point problem of $[\text{Al}/\text{H}]$ seen in the old LTE work be removed by including the non-LTE corrections? Are the non-LTE abundances derived from 3944 and 3961 lines consistent with each other?
- Possibilities of Al abundance determination based on the other lines (than the Al I resonance lines of primary concern) are also examined, such as Al I 6696/6698 lines (used by Burkhart and Coupry) or Al II 3900/4663 lines (which have barely been employed in A-type stars). How are the non-LTE corrections for these lines?

2. Non-LTE calculation for Al

2.1. Atomic model and computational details

The statistical-equilibrium calculations for aluminium were carried out by using the non-LTE code described in Takeda (1991). The atomic model of Al adopted in this study was constructed based on Kurucz and Bell's (1995) compilation of atomic data (gf values, levels, etc.), which consists of 65 Al I terms (up to $26s^2S$ at 48092 cm^{-1}) with 218 Al I radiative transitions, 68 Al II terms (up to $10p^3P^o$ at 146602 cm^{-1}) with 601 Al II radiative transitions, and 32 Al III terms (up to $9h^2H^o$ at 217252 cm^{-1} ; included only for conservation of total Al atoms). The ground $^2P^o$ term of Al I (comprising two closely lying levels with statistical weights of $g = 2$ and 4 corresponding to $J = 1/2$ and $3/2$) was treated as a single level with $g = 6$.

Regarding the calculation of photoionization rates, the cross-section data taken from the TOPbase (Cunto, Mendoza 1992) were used for the lower 10

Al I terms and 10 Al II terms (while hydrogenic approximation was assumed for all other higher terms). As to the collisional (excitation and ionization) rates due to electron as well as neutral hydrogen, the recipe described in Sect. 3.1.3 of Takeda (1991) was followed. Inelastic collisions due to neutral hydrogen atoms were formally included by the analytical formula as described therein with a moderate scaling factor of $S_{\text{H}} = 0.4$ by following Steenbock and Holweger (1992) as well as Baumüller and Gehren (1997), though the effect of neutral hydrogen collision is insignificant in the atmosphere of early-type stars ($T_{\text{eff}} \gtrsim 7000$ K) under question.

The calculations were done on a grid of 192 ($= 12 \times 4 \times 4$) Kurucz's (1993) ATLAS9 models atmospheres (scaled solar-abundance models according to the metallicity $[\text{Fe}/\text{H}]$) resulting from combinations of twelve T_{eff} values (6500, 7000, 7500, 8000, 8500, 9000, 9500, 10000, 11000, 12000, 13000, and 14000 K) and four $\log g$ values (3.0, 3.5, 4.0, and 4.5), and four $[\text{Fe}/\text{H}]$ values (-1.0 , -0.5 , 0.0 , and $+0.5$) while assuming $\xi = 2 \text{ km s}^{-1}$ (microturbulence) and metallicity-scaled abundances of $A(\text{Al}) = 6.47 + [\text{Fe}/\text{H}]$ (where 6.47 is the solar Al abundance used in Kurucz's ATLAS9 models) were adopted as the input Al abundance.

2.2. Behaviors of non-LTE departure coefficients

The non-LTE departure coefficients of the representative four Al terms calculated for the model corresponding to Vega are plotted against the optical depth in Fig. 3. Comparing this figure with Fig. 2 of Steenbock and Holweger (1992), we can see that both calculations are reasonably consistent with each other.

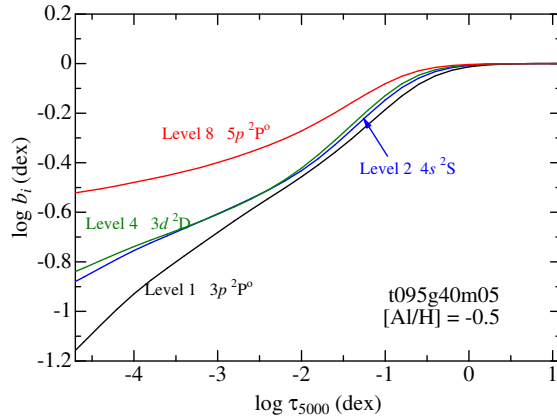


Figure 3. Run of the non-LTE departure coefficients ($b_i \equiv n_i^{\text{NLTE}}/n_i^{\text{LTE}}$) of neutral Al atom with the continuum optical depth at 5000 \AA calculated for the model of $T_{\text{eff}} = 9500$ K, $\log g = 4.0$, and $[\text{M}/\text{H}] = [\text{Fe}/\text{H}] = [\text{Al}/\text{H}] = -0.5$. Shown here are the results for the selected lower 4 terms of $3p^2\text{P}^o$, $4s^2\text{S}$, $3d^2\text{D}$, and $5p^2\text{P}^o$ ($i = 1, 2, 4$, and 8). This figure is arranged so as to be compared with Steenbock and Holweger's (1992) Fig. 2.

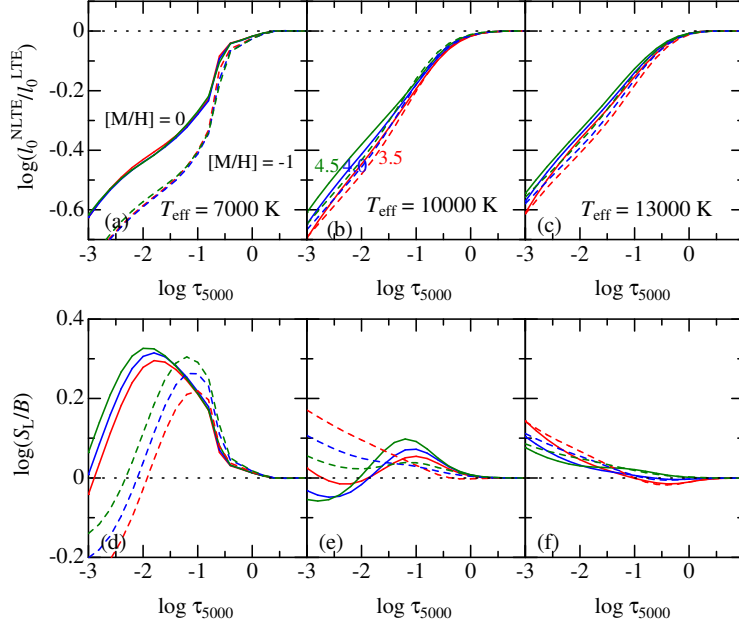


Figure 4. The non-LTE-to-LTE line-center opacity ratio (upper panels a–c) and the ratio of the line source function (S_L) to the local Planck function (B) (lower panels d–f) for the Al I $3p^2P^o-4s^2S$ transition (corresponding to Al I 3944/3961 lines) of multiplet 1, plotted against the continuum optical depth at 5000 Å. Shown here are the calculations done with $\xi = 2 \text{ km s}^{-1}$ on the solar-metallicity models ($[M/H] = [Fe/H] = 0$; solid lines) and $1/10\times$ metal-deficient models ($[M/H] = [Fe/H] = -1$; dashed lines) of $T_{\text{eff}} = 7000 \text{ K}$ (left panels a, d), 10000 K (middle panels b, e), and 13000 K (right panels c, f), where metallicity-scaled Al abundance ($[Al/Fe] = 0$) was adopted in the calculation. At each panel, the results for three $\log g$ values of 3.5, 4.0, and 4.5 are depicted by different colors (red, blue, and green, respectively).

Fig. 4 also shows the $l_0^{\text{NLTE}}(\tau)/l_0^{\text{LTE}}(\tau)$ (the non-LTE-to-LTE line-center opacity ratio; almost equal to $\simeq b_1$) and $S_L(\tau)/B(\tau)$ (the ratio of the line source function to the Planck function; nearly equal to $\simeq b_2/b_1$) for the transition relevant to the Al I 3944/3961 lines (b_1 and b_2 are the non-LTE departure coefficients for the lower and upper terms), which were computed on the models of representative T_{eff} and $\log g$ values.

As seen from this figure, the inequality relation $l_0^{\text{NLTE}}/l_0^{\text{LTE}} < 1$ (underpopulation or overionization) prevails in all depths, and the relation $S_L/B \gtrsim 1$ (enhancement of the line source function) tends to hold in the line-forming region, both acting in the direction of weakening the strengths of absorption lines. Therefore, the Al I resonance doublet lines at 3944/3961 Å are weakened

by the non-LTE effect. Since this non-LTE underpopulation is due to the overionization mechanism caused by the imbalance between the photoionization and photorecombination rates ($J > B$), its extent may be sensitive to the metallicity ($[M/H]$) which generally plays an important role for the UV radiation field. According to Fig. 4, however, the effect of changing $[M/H]$ is not so significant except for the case of lower T_{eff} (7000 K).

Table 1. Adopted atomic data of Al lines.

Species	Multiplet No.	λ (Å)	χ_{low} (eV)	$\log gf$ (dex)	Gammar (dex)	Gammas (dex)	Gammaw (dex)
Al I	1	3944.006	0.000	-0.623	(8.16)	(-6.30)	-7.32
Al I	1	3961.520	0.014	-0.323	(8.16)	(-6.30)	-7.32
Al I	5	6696.023	3.143	-1.347	(7.70)	(-5.16)	(-7.28)
Al I	5	6698.673	3.143	-1.647	(7.70)	(-5.16)	(-7.28)
Al II	1	3900.675	7.421	-1.270	9.22	(-5.95)	(-7.77)
Al II	2	4663.046	10.598	-0.284	7.99	(-5.53)	(-7.64)

Note.

These data are were taken from the VALD database (Ryabchikova et al. 2015), while those parenthesized are the default values calculated by Kurucz's (1993) WIDTH9 program.

Followed by first five self-explanatory columns, damping parameters are given in the last three columns:

Gammar is the radiation damping width (s^{-1}), $\log \gamma_{\text{rad}}$.

Gammas is the Stark damping width (s^{-1}) per electron density (cm^{-3}) at 10^4 K, $\log(\gamma_e/N_e)$.

Gammaw is the van der Waals damping width (s^{-1}) per hydrogen density (cm^{-3}) at 10^4 K, $\log(\gamma_w/N_H)$.

2.3. Grid of abundance corrections

Based on the results of these calculations, theoretical equivalent-widths and the corresponding non-LTE abundance corrections for Al I 3944 and 3961 lines were computed for each of the models as follows. First, for an assigned Al abundance ($A = 6.47 + [\text{Fe}/\text{H}]$) and microturbulence (ξ ; any of 1, 2, 3, and 4 km s^{-1}),³ the non-LTE equivalent width (W^{N}) of the line was calculated by using the computed non-LTE departure coefficients (b) for each model atmosphere (LTE equivalent width W^{L} was also calculated for comparison, though not used for evaluation of Δ). Next, the LTE (A^{L}) and NLTE (A^{N}) abundances were computed from this W^{N} while regarding it as if being a given observed equivalent width. We could then obtain the non-LTE abundance correction (Δ), which is defined in terms of these two abundances as $\Delta \equiv A^{\text{N}} - A^{\text{L}}$.

Here, Kurucz's (1993) WIDTH9 program, which was considerably modified in many respects (e.g., incorporation of non-LTE departure in the line source function as well as in the line opacity, etc.), was employed for calcu-

³The departure coefficients computed for a fixed ξ of 2 km s^{-1} were applied also to the cases of $\xi = 1, 3,$ and 4 km s^{-1} because they are not so sensitive to a choice of ξ .

lating the equivalent width for a given abundance, or inversely evaluating the abundance for an assigned equivalent width. The background opacities of overlapping Balmer lines, which are important for these Al lines in the violet region (especially for the 3961 line), were included as done in Kurucz’s (1993) ATLAS9 program (Griem 1960, 1967). The adopted atomic data of these lines (gf values, damping constants, etc.) are summarized in Table 1. The resulting grids of W^L , W^N , A^N , A^L , and Δ calculated for 3944 and 3961 lines are presented in the supplementary materials: 8 data files named as “ncor####.%%”, where ‘####’ denotes the relevant line (‘3944’ or ‘3961’) and ‘%%’ is the metallicity code (‘m10’, ‘m05’, ‘p00’, and ‘p05’ corresponding to $[X/H] = [Fe/H] = -1.0$, -0.5 , 0.0 , and $+0.5$, respectively).

2.4. Dependence of W and Δ upon stellar parameters

How the theoretical W and Δ computed for these two Al I lines depend upon the atmospheric parameters (T_{eff} , $\log g$, and ξ) is illustrated in Fig. 5, from which the following characteristics are read.

- The equivalent widths (W) progressively decrease with an increase in T_{eff} , reflecting the T -dependence of $\propto \exp[\chi_{\text{ion}}/(kT)]$ for the number population of the ground level (k is the Boltzmann constant, χ_{ion} is the ionization potential of 5.98 eV), while the inequality relation of $W^N < W^L$ (non-LTE line weakening) generally holds if compared at the same condition. Although the transition probability (gf value) for the 3961 line is twice as stronger as that of the 3944 line (cf. Table 1), the difference between W_{3944} and W_{3961} is not so manifest, which is presumably because the latter W_{3961} is more significantly affected by the opacity of He I line wing (tending to weaken the line strength).
- The non-LTE corrections are always positive ($\Delta > 0$) reflecting that the line is weakened by the non-LTE effect, and significantly large (~ 0.2 – 1.0 dex). The Δ values appreciably depend upon W (and thus upon T_{eff}), tending to be larger with increasing W . This is because the line-forming region moves towards the upper layer (where the departure from LTE is more significant) until desaturation begins in the flat-to-damping transition part of the curve of growth ($W \gtrsim 200$ mÅ at $T_{\text{eff}} \lesssim 8000$ K). Generally, Δ_{3944} is smaller than Δ_{3961} , because the latter 3961 line (larger opacity) forms in a comparatively higher layer.
- W tends to decline with a decrease in $\log g$, because ionization is enhanced in the condition of lowered density. Since these lines are generally strong ($W \gtrsim 100$ mÅ) as to be in the flat part of the curve of growth, W sensitively grows with an increase in ξ . The reason why Δ tends to increase with $\log g$ as well as ξ can be understood in terms of the W -dependence of Δ mentioned above.

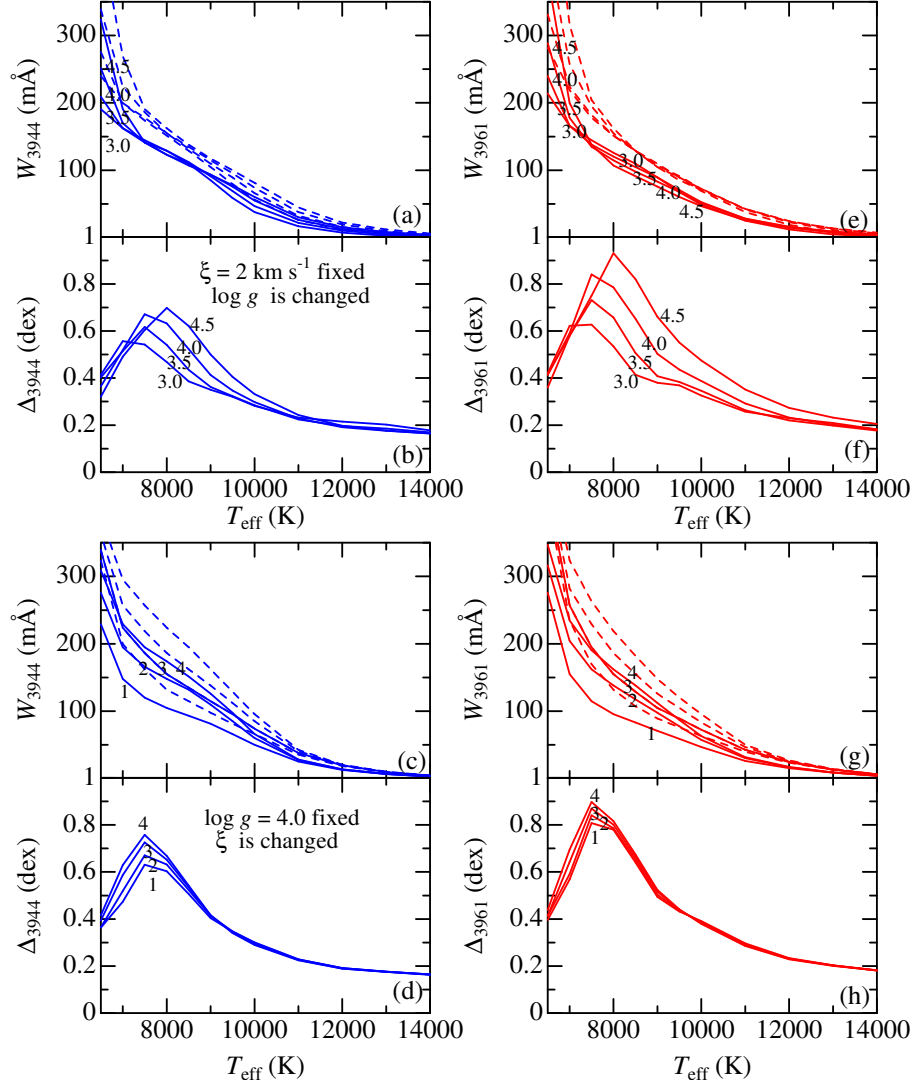


Figure 5. The non-LTE and LTE equivalent widths (W^{N} and W^{L}) for the Al I 3944/3961 lines and the corresponding non-LTE corrections (Δ), which were computed on the non-LTE grid of models described in Sect 2.1, are plotted against T_{eff} . Each figure set consists of two panels; the upper panel is for W^{N} (solid lines) and W^{L} (dashed lines), while the lower panel is for Δ . The upper sets (a+b, e+f) show the case of fixed ξ (2 km s^{-1}) but different $\log g$ (3.0, 3.5, 4.0, and 4.5), while the lower sets (c+d, g+h) are for the case of fixed $\log g$ (4.0) but different ξ (1, 2, 3, and 4 km s^{-1}). The left-hand figures show the results for the Al I 3944 line, while the right-hand ones for the Al I 3961 line.

3. Analysis of Al I 3944/3947 lines for A-type stars

3.1. Observational data

Our next task is to determine the Al abundances for a number of sample stars from the Al I resonance doublet lines at 3944 and 3961 Å by taking into account the non-LTE effect. Regarding the observational data for this purpose, Takeda et al.’s (2008, 2009) spectra of A-type stars obtained by BOES (Bohunsan Observatory Echelle Spectrograph) were mainly used (Group B in Table 2), because they cover the relevant violet region thanks to their wide wavelength coverage, where stars are limited to those of low-to-moderate projected rotational velocities ($v_e \sin i \leq 100 \text{ km s}^{-1}$) as done in Takeda et al. (2018) or Takeda (2022).

In addition, the spectra of 7 sharp-lined particularly bright A-type stars were secured by new observations specifically directed to the shorter wavelength region (Group A in Table 2), which were carried out on 2016 November 2–6 at the Okayama Astrophysical Observatory by using the 188 cm reflector along with HIDES (HIGH Dispersion Echelle Spectrograph) in the mode of a blue cross disperser. The data reduction was done in the standard manner by using IRAF,⁴ by which the spectra covering 3300–5600 Å with a resolving power of $R \sim 100000$ were obtained. The finally resulting 63 program stars (7 from Group A and 56 from Group B) are listed in Table 3.

It should be remarked here that a fraction of the Group B spectra (9 stars) may be problematic in the sense that lines in the short-wavelength region appear unusually weaker than expected (designated as “stars with weak broad Ca II K line” in Takeda 2020). Since different echelle orders are closely packed and the count level is considerably low in the blue-violet region of BOES spectra, this effect might be due to the stray light within the spectrograph. Accordingly, the results derived for those stars (marked with parentheses and asterisks in Table 3) should be viewed with caution.

Table 2. Basic information of the adopted observational data.

Group	Instr.	Obs. Time	Resolution	Applied lines	Reference
A	HIDES	2017 Oct	100000	3944/3961/ /3900/4663	see Sect. 3.1
B	BOES	2008 Jan/Sep, 2009 Jan	45000	3944/3961/6696/ /6698/4663	Takeda et al. (2008, 2009)
C	HIDES	2008 Oct	100000	6696/6698/4663	Takeda et al. (2012)
D	HIDES	2006 May	100000	4663	Takeda et al. (2007)

The group, to which the observational data adopted for each star belongs, is indicated in Table 3/tableE1.dat (3944/3961 lines; A or B), tableE2.dat (6696/6698 lines; B or C), tableE3.dat (3900 line; A), and tableE4.dat (4663 line; A or B or C or D).

⁴ IRAF is distributed by the National Optical Astronomy Observatories, which is operated by the Association of Universities for Research in Astronomy, Inc. under cooperative agreement with the National Science Foundation.

Table 3. Program stars and their atmospheric parameters.

HD# (1)	Name (2)	Sp.Type (3)	T_{eff} (4)	$\log g$ (5)	[Fe/H] (6)	ξ (7)	$v_e \sin i$ (8)	Group (9)	SB/V (10)	CP (11)	Hyades (12)
018454	4 Eri	A5IV/V	7740	4.07	+0.24	3.9	100	B	V		
076543	σ^1 Cnc	A5III	8330	4.18	+0.38	3.9	91	B	SB		
012216	50 Cas	A2V	9553	3.90	+0.15	2.6	88	B	SB2		
028355	79 Tau	A7V	7809	3.98	+0.19	4.0	87	B	V?		H
222345	ω^1 Aqr	A7IV	7487	3.88	-0.07	3.8	86	B	SB		
074198	γ Cnc	A1IV	9381	4.11	+0.25	2.8	85	B	SB		
027934	κ^1 Tau	A7IV-V	8159	3.84	+0.02	4.0	83	B	SB?		H
025490	ν Tau	A1V	9077	3.93	-0.05	3.2	82	B			
029388	90 Tau	A6V	8194	3.88	-0.01	4.0	82	B	SB1		H
079469	θ Hya	B9.5V	10510	4.20	-0.02	1.4	82	B	SB		
028226		Am	7361	4.01	+0.31	3.6	81	B	SB2	Am	H
207098	δ Cap	A5mF2 (IV)	7312	4.06	+0.21	3.6	81	B	SBo	Am	
033641	μ Aur	A4m	7961	4.21	+0.18	4.0	79	B	V	Am	
216627	δ Aqr	A3V	8587	3.59	-0.25	3.7	79	B	V		
012111	48 Cas	A3IV	7910	4.08	-0.23	4.0	76	B	SBo		
(*023281)		A5m	7761	4.19	+0.05	4.0	76	B		Am	
192640	29 Cyg	A2V	8845	3.86	-1.41	3.5	74	B	V	λ Boo	
011636	β Ari	A5V...	8294	4.12	+0.15	3.9	73	B	SBo		
005448	μ And	A5V	8147	3.82	-0.14	4.0	72	B			
173880	111 Her	A5III	8567	4.27	+0.22	3.8	72	B	SB?		
017093	38 Ari	A7III-IV	7541	3.95	-0.23	3.8	69	B	V		
028319	θ^2 Tau	A7III	7789	3.68	-0.13	4.0	68	B	SB1o		H
095382	59 Leo	A5III	8017	3.95	-0.09	4.0	68	B			
(*140436)	γ CrB	A1Vs	9274	3.89	-0.27	3.0	68	B			
020320	ζ Eri	A5m	7505	3.91	-0.12	3.8	67	B	SBo	Am	

Table 3. Continued.

HD# (1)	Name (2)	Sp.Type (3)	T_{eff} (4)	$\log g$ (5)	[Fe/H] (6)	ξ (7)	$v_e \sin i$ (8)	Group (9)	SB/V (10)	CP (11)	Hyades (12)
013161	β Tri	A5III	7957	3.68	-0.32	4.0	65	B	SB2o		
027045	ω^2 Tau	A3m	7552	4.26	+0.36	3.8	62	B	SB	Am	
200499	η Cap	A5V	8081	3.95	-0.17	4.0	62	B	V		
(*029499)		A5m	7638	4.08	+0.29	3.9	61	B	V	Am	H
116656	ζ UMa	A2V	9317	4.10	+0.28	2.9	59	B	SB2o		
198639	56 Cyg	A4me...	7921	4.09	+0.02	4.0	59	B	V?	Am	
(*130841)	α^2 Lib	A3IV	8079	3.96	-0.24	4.0	58	B	SB		
030121	4 Cam	A3m	7700	3.98	+0.27	3.9	57	B		Am	
029479	σ^1 Tau	A4m	8406	4.14	+0.35	3.9	56	B	SBo	Am	H
030210		Am...	7927	3.94	+0.40	4.0	56	B	SB1?	Am	H
222603	λ Psc	A7V	7757	3.99	-0.17	4.0	56	B	SB		
212061	γ Aqr	A0V	10384	3.95	-0.08	1.5	54	B	SB		
089021	λ UMa	A2IV	8861	3.61	+0.08	3.5	52	B	V		
195725	θ Cep	A7III	7816	3.74	+0.16	4.0	49	B	SB2o		
043378	2 Lyn	A2Vs	9210	4.09	-0.15	3.0	46	B	V?		
027819	δ^2 Tau	A7V	8047	3.95	-0.05	4.0	45	B	SB		H
095418	β UMa	A1V	9489	3.85	+0.24	2.7	44	B	SB		
(*218396)		A5V	7091	4.06	-0.59	3.3	41	B			
084107	15 Leo	A2IV	8665	4.31	+0.01	3.7	38	B			
204188		A8m	7622	4.21	+0.02	3.9	36	B	SBo	Am	
(*033204)		A5m	7530	4.06	+0.18	3.8	34	B		Am	H
141795	ϵ Ser	A2m	8367	4.24	+0.25	3.9	32	B	V	Am	
173648	ζ^1 Lyr	Am	8004	3.90	+0.32	4.0	32	B	SB1o	Am	
(*027628)	60 Tau	A3m	7218	4.05	+0.10	3.5	30	B	SB1o	Am	H

Table 3. Continued.

HD# (1)	Name (2)	Sp.Type (3)	T_{eff} (4)	$\log g$ (5)	[Fe/H] (6)	ξ (7)	$v_e \sin i$ (8)	Group (9)	SB/V (10)	CP (11)	Hyades (12)
028546	81 Tau	Am	7640	4.17	+0.23	3.9	28	B	V?	Am	H
182564	π Dra	A2III _s	9125	3.80	+0.39	3.1	27	A			
172167	α Lyr	A0Vvar	9435	3.99	-0.53	2.7	22	A	V	λ Boo?	
060179	α Gem	A2Vm	9122	3.88	-0.02	3.2	19	B	SB1 _o	Am	
058142	21 Lyn	A1V	9384	3.74	-0.05	2.8	19	A	V		
095608	60 Leo	A1m	8972	4.20	+0.31	3.3	18	B		Am	
048915	α CMa	A0m...	9938	4.31	+0.45	2.1	17	A	SBo	Am	
(*027749)	63 Tau	A1m	7448	4.21	+0.41	3.7	13	B	SB1 _o	Am	H
(*033254)	16 Ori	A2m	7747	4.14	+0.28	3.9	13	B	SBo	Am	H
072037	2 UMa	A2m	7918	4.16	+0.19	4.0	12	B		Am	
040932	μ Ori	Am...	8005	3.93	-0.12	4.0	11	B	SB1 _o	Am	H
027962	δ^3 Tau	A2IV	8923	3.94	+0.25	3.4	11	A	SB		H
047105	γ Gem	A0IV	9115	3.49	-0.03	3.2	11	A	SB		
214994	<i>o</i> Peg	A1IV	9453	3.64	+0.18	2.7	6	A	V		

(1) HD number. Regarding those parenthesized with asterisks (9 stars), caution should be taken because their observational data may be unreliable (cf. Sect. 3.1). (2) Bayer/Flamsteed name. (3) Spectral type taken from Hipparcos catalogue (ESA 1997). (4) Effective temperature (in K). (5) Logarithmic surface gravity ($\log g$ in dex, where g is in unit of cm s^{-2}). (6) Differential Fe abundance relative to Procyon (\simeq Sun) derived as $A(\text{Fe}) - 7.49$. (7) Microturbulent velocity (in km s^{-1}). (8) Projected rotational velocity (in km s^{-1}). (9) Data source group used for the analysis of Al I 3944/3961 lines (cf. Table 2). (10) Key to spectroscopic binary (SB, “o” denotes the case where orbital elements are available) or radial velocity variable (V). (11) Key to chemical peculiarity type (Am or λ Boo), where the spectral classifications in three sources were consulted: Hipparcos catalogue (ESA 1997), Bright Star Catalogue (Hoffleit, Jaschek 1991), and SIMBAD. (12) Key to membership of Hyades cluster (H). Since these data (arranged in the descending order of $v_e \sin i$) are essentially the subset of those used in Takeda et al. (2018), the caption of Table 1 of that paper may be consulted for more details.

3.2. Atmospheric parameters

The atmospheric parameters of the program stars are presented in Table 3, which are the same as determined and adopted in Takeda et al. (2008, 2009). Since only brief descriptions are given here, these papers should be consulted for more details: T_{eff} and $\log g$ are from Strömgren’s $uvby\beta$ color indices by using Napiwotzki et al.’s (1993) calibration, ξ is from the empirical T_{eff} -dependent relation [cf. Eq.(1) of Takeda et al. 2008], and $[\text{Fe}/\text{H}]$ (Fe abundance, representative of the metallicity) is from the spectrum fitting analysis in the 6140–6170 Å region.

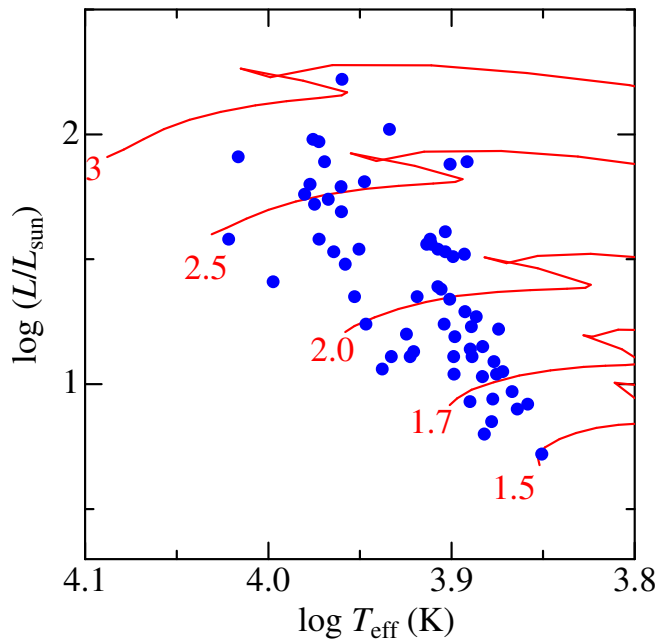


Figure 6. Our program stars plotted on the $\log(L/L_{\odot})$ vs. $\log T_{\text{eff}}$ diagram, where L (luminosity) was evaluated from visual magnitude (corrected for interstellar extinction by following Arenou et al. 1992), Hipparcos parallax (van Leeuwen 2007), and bolometric correction (Flower 1996). Lejeune and Schaerer’s (2001) theoretical solar-metallicity tracks for 5 different masses (1.5, 1.7, 2, 2.5, and 3 M_{\odot}) are also depicted by solid lines for comparison.

The model atmosphere for each star was generated by interpolating Kurucz’s (1993) ATLAS9 grid of models in terms of T_{eff} , $\log g$, and $[\text{Fe}/\text{H}]$. Likewise, the depth-dependent non-LTE departure coefficients to be used for each of the program stars were obtained by interpolation of the calculated grids (Sect. 2.1) with respect to T_{eff} , $\log g$, and $[\text{Fe}/\text{H}]$.

The 63 program stars are plotted on the $\log T_{\text{eff}}$ vs. $\log L$ diagram in Fig. 6, where the theoretical evolutionary tracks of different masses are also depicted for comparison. We can see from this figure that these stars are in the mass range of $1.5M_{\odot} \lesssim M \lesssim 3M_{\odot}$.

3.3. Abundance determination

The abundances of Al for each of the 63 stars were determined in the similar manner as done in the previous papers (Takeda et al. 2008, 2009, 2018; Takeda 2022). (i) First, Takeda’s (1995) spectrum-fitting technique is applied to each of the spectral regions comprising Al I 3944 and 3961 lines, while varying several free parameters ($v_e \sin i$, radial velocity, and abundances of important elements; see Table 4 for more information), and the best fit parameter solutions are determined. (ii) Then, based on such established abundance solutions, the equivalent widths of these two Al lines (W) were inversely calculated. (iii) Finally, non-LTE (A^{N}) and LTE (A^{L}) abundances were derived from W , along with the corresponding non-LTE correction $\Delta (\equiv A^{\text{N}} - A^{\text{L}})$. The accomplished fit between the theoretical and observed spectra is displayed for each region in Fig. 7, and the results of the analysis (W , A^{N} , A^{L} , Δ) for each line are summarized in “tableE1.dat” of the supplementary materials.

Table 4. Details of spectrum fitting analyses.

Lines	Fitting (\AA) range (\AA)	Abundances varied*	Targets	Figure
Al I 3944	3941.5–3946.5	Al, Fe	All 63 stars	Fig. 7
Al I 3961	3859–3964	Al, Fe	All 63 stars	Fig. 7
Al I 6696/6698	6692–6701	Al, Fe	8 sharp-lined late-A stars	Fig. 11a
Al II 3900	3898.5–3902	Al, Ti, V, Fe	6 sharp-lined early-A stars	Fig. 11c
Al II 4663	4662–4665	Al, Fe	10 sharp-lined early-A stars	Fig. 11e

* The abundances of other elements than these were fixed by assuming $[X/H] = [\text{Fe}/H]$ in the fitting.

The resulting W_{3944} , Δ_{3944} , and A_{3944}^{N} along with the abundance sensitivities to typical ambiguities in atmospheric parameters [$\delta_{T_{\pm}}$ (abundance changes for T_{eff} perturbations by $\pm 3\%$), $\delta_{g_{\pm}}$ (abundance changes for $\log g$ perturbations by ± 0.1 dex), and $\delta_{\xi_{\pm}}$ (abundance changes for ξ perturbations by $\pm 30\%$)] are plotted against T_{eff} in Fig. 8. (Although the results only for the Al I 3944 line are shown here, those for the 3961 line are quite similar.) Fig. 8a and 8b confirm the trends of W and Δ already described in Sect. 2.4. It can be seen also from Fig. 8d and 8f that Al abundances derived from these strong resonance lines are quite sensitive to T_{eff} and especially to ξ , as expected.

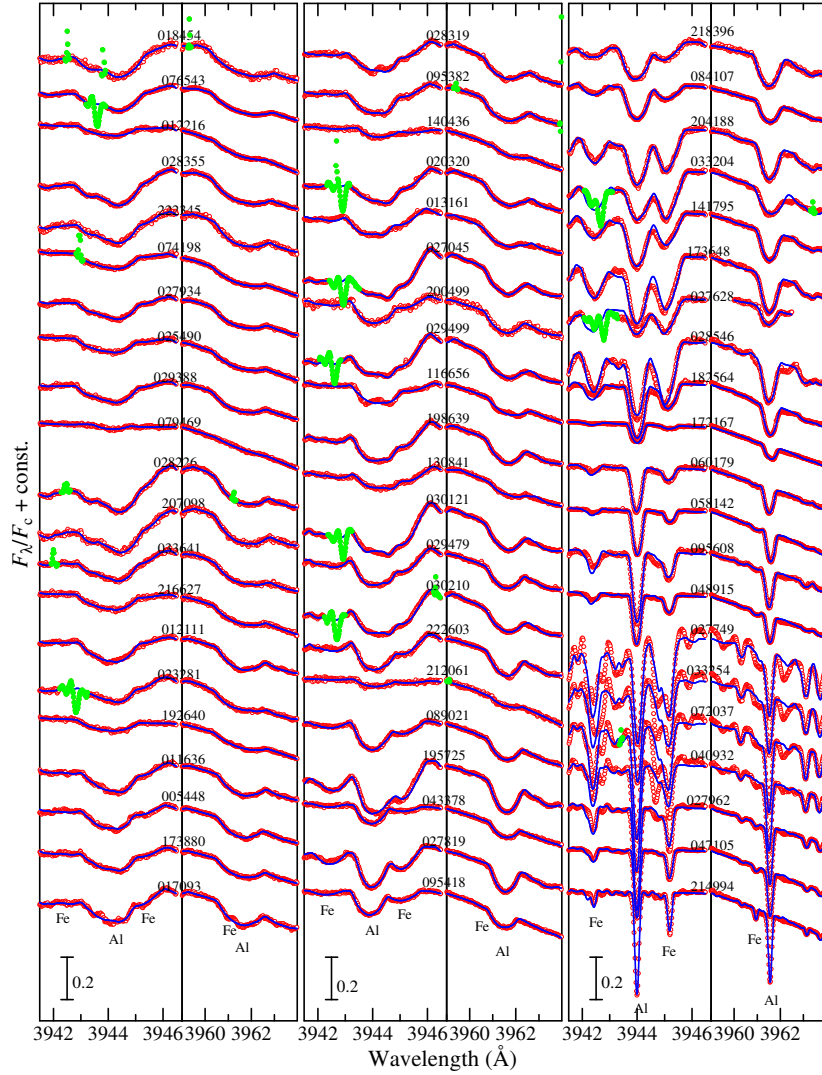


Figure 7. Synthetic spectrum-fitting analysis for Al abundance determinations from Al I 3944/3961 lines. The best-fit theoretical spectra (in the selected ranges of 3941.5–3946.5 Å and 3959–3964 Å comprising the relevant Al I lines) are depicted by blue solid lines, while the observed data are plotted by red symbols (the masked data excluded in judging the goodness of the fit are highlighted in green). In each panel, the spectra (residual fluxes F_λ/F_c ; the spectrum at 3946.5 Å in the left and that at 3959 Å in the right) are so adjusted as to coincide with each other. An appropriate offset is applied to each spectrum (indicated by the HD number) relative to the adjacent one. The wavelength scale is in the laboratory frame after correcting the radial velocity shift.

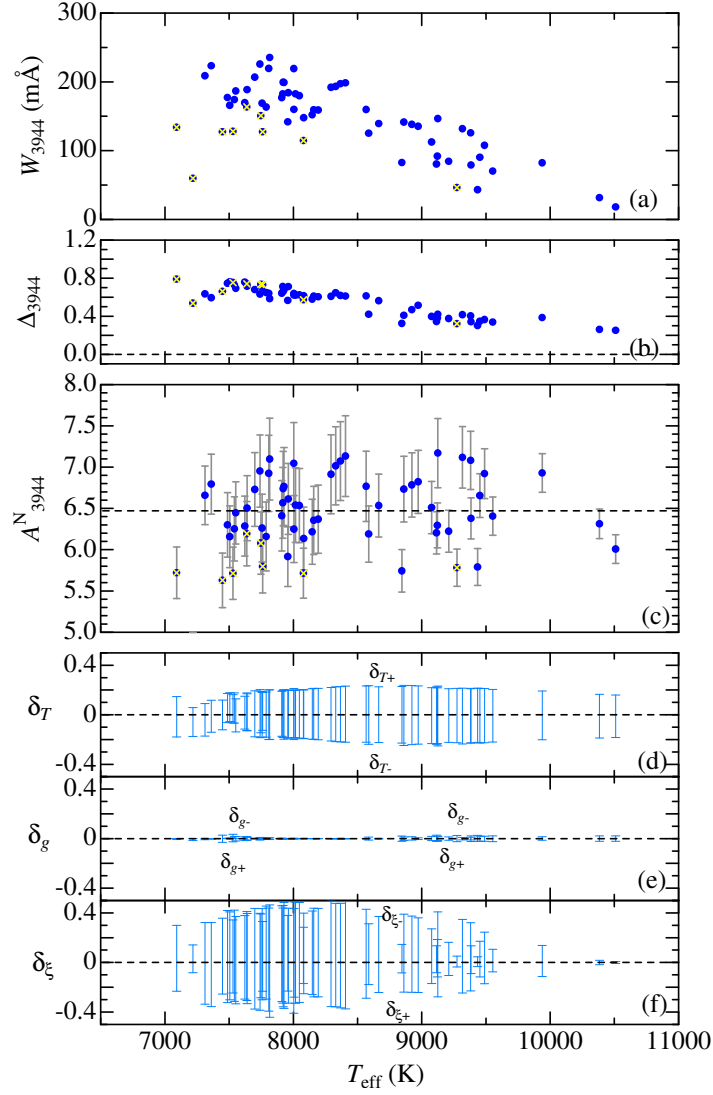


Figure 8. Al abundances and the related quantities of the program stars, which were derived from the Al I 3944 line, are plotted against T_{eff} . (a) Equivalent widths (W_{3944} , filled symbols). (b) Non-LTE corrections (Δ_{3944} , filled symbols). (c) A_{3944}^N (non-LTE Al abundances), where the adopted solar abundance ($A_{\odot} = 6.47$) is indicated by the horizontal dashed line and the error bar denotes $\pm\delta_{Tgv}$ defined as the root-sum-square of δ_T , δ_g , and δ_{ξ} (e.g., δ_T is the mean of $|\delta_{T+}|$ and $|\delta_{T-}|$; etc.). (d) δ_{T+} and δ_{T-} (abundance variations in response to T_{eff} changes of +3% and -3%). (e) δ_{g+} and δ_{g-} (abundance variations in response to $\log g$ changes by +0.1 dex and -0.1 dex). (f) $\delta_{\xi+}$ and $\delta_{\xi-}$ (abundance variations in response to perturbing ξ by +30% and -30%). The results based on unreliable observational data (cf. Sect. 3.1) are distinguished by overplotting yellow crosses in panels (a)–(c).

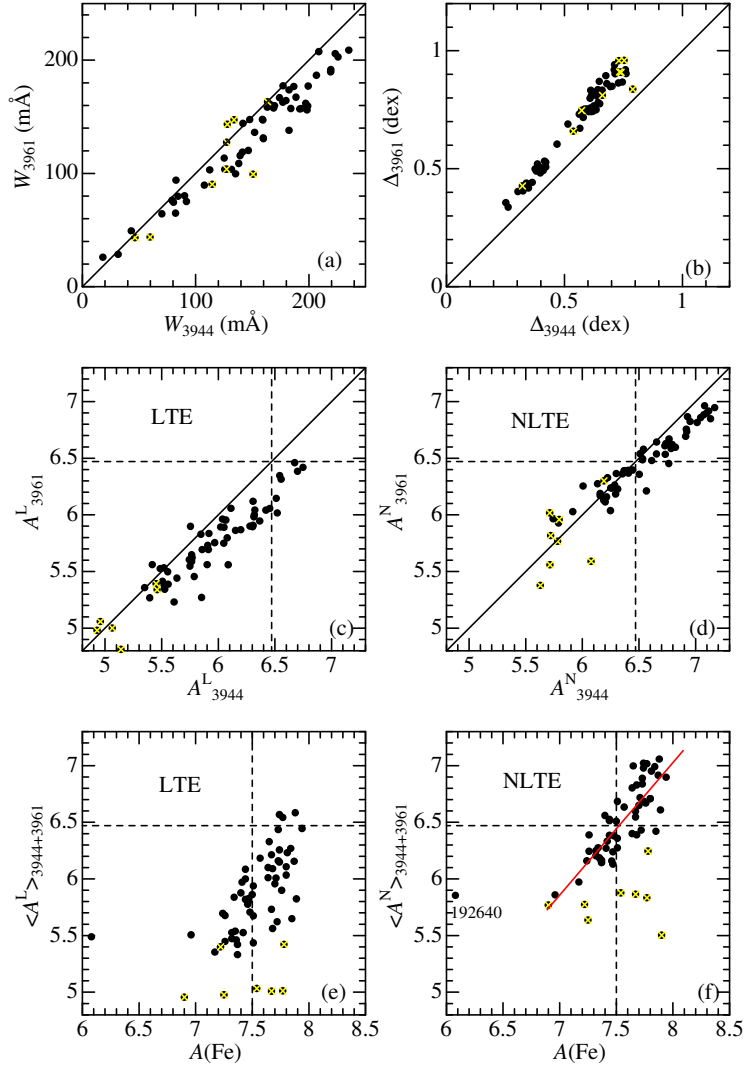


Figure 9. Panels (a)–(d) show the correlations of the quantities between Al I 3944 and 3961 lines (a: equivalent widths, b: NLTE corrections, c: LTE abundances, and d: NLTE abundances). The mean Al abundances derived from Al I 3944/3961 lines, defined as $\langle A \rangle_{3944+3961} \equiv (A_{3944} + A_{3961})/2$, are plotted against $A(\text{Fe})$ ($= [\text{Fe}/\text{H}] + 7.49$; cf. Table 1) in panel (e; LTE) and panel (f; NLTE). The results based on unreliable observational data (cf. Sect. 3.1) are distinguished by overplotting yellow crosses as in Fig. 8. In each panel, the locations of solar abundances are indicated by dashed lines. The solid line in panels (a)–(d) is the guide line corresponding to $X_{3944} = X_{3961}$ (X is Δ or A), while the red solid line depicted in panel (f) is the linear-regression line showing the main trend (cf. Sect. 3.4).

3.4. Results and their characteristics

The abundances and related quantities resulting from the analysis of the Al I 3944/3961 lines are graphically depicted in Fig. 9, from which the following trends are observed.

- While the equivalent widths of these doublet lines (W_{3944} and W_{3961}) are not much different from each other (Fig. 9a), the non-LTE corrections generally satisfy the inequality relation ($0 < \Delta_{3944} < \Delta_{3961}$) (Fig. 9b), as already mentioned in Sect. 2.4.
- Although A_{3944}^L tends to be systematically higher than A_{3961}^L in the LTE case (Fig. 9c), this discrepancy is mitigated by the difference in Δ to result in $A_{3944}^N \approx A_{3961}^N$ in the non-LTE case (Fig. 9d).
- In terms of the averaged abundance between two lines, $\langle A \rangle_{3944+3961} \equiv (A_{3944} + A_{3961})/2$, while the LTE abundances ($\langle A^L \rangle_{3944+3961}$) are considerably subsolar around the solar metallicity (Fig. 9e), this discordance is satisfactorily removed in the non-LTE case ($\langle A^N \rangle_{3944+3961}$), so that normal-metallicity stars reasonably show $A_{\text{star}} \sim A_{\odot}$ for both Al and Fe (Fig. 9f).
- By applying the least-squares analysis to the data in Fig. 9f (while excluding those yellow-crossed unreliable ones and that of the λ Boo star HD 192640 showing exceptionally low metallicity of $[\text{Fe}/\text{H}] = -1.41$), the linear-regression relation $[\text{Al}/\text{H}] = 1.17(\pm 0.11) [\text{Fe}/\text{H}] - 0.04(\pm 0.03)$ is obtained, where $[\text{Al}/\text{H}] = A(\text{Al}) - 6.47$ and $[\text{Fe}/\text{H}] = A(\text{Fe}) - 7.49$.
- The scaling relation ($[\text{Al}/\text{H}] \sim 1.2 [\text{Fe}/\text{H}]$) observationally established here indicates that an overabundance of Al is associated with an increased Fe abundance in the surface of A-type stars. This trend is qualitatively consistent with the prediction from the diffusion theory, which suggests an abundance excess of Al (like Fe) as a result of the element segregation process in the envelope of Am stars (Richer et al. 2000; Talon et al. 2006).

3.5. Interpretation of the problems in previous studies

It is now possible to discuss the problematic issues seen in the old Al abundance determinations for A-type stars based on the Al I resonance doublet lines.

The serious zero-point discrepancy in $[\text{Al}/\text{H}]$ (considerably negative $[\text{Al}/\text{H}]$ values for $[\text{Fe}/\text{H}] \sim 0$ stars) seen in the Al abundances derived from Al I 3944/3961 lines by Smith (1971, 1973) and Adelman (et al.) in 1980s–90s (cf. Figs. 2a and 2c) is simply because they adopted LTE in their analysis. Since appreciable (positive) non-LTE corrections due to Al I overionization are required, LTE Al abundances are significantly underestimated and shifted towards subsolar direction (Fig. 9e). This problem can be reasonably resolved by taking into account the non-LTE effect as shown in Fig. 9f.

The systematic discrepancy in the LTE abundances between Al I 3944 and 3961 lines seen in Adelman et al.'s results ($A_{3944} > A_{3961}$; cf. Fig. 2d) may also be associated to the non-LTE effect, because neglecting non-LTE corrections ($\Delta_{3944} < \Delta_{3961}$) results in such a tendency as shown in Fig. 9c. However, the extent of discordance observed in Fig. 2d seems to be larger than that expected from Fig. 9c. As another possibility, they might have not included the opacity of Balmer line wings, the neglect of which can cause appreciable abundance differences because the 3961 line is more affected by this effect (due to H ϵ at 3970 Å) than the 3944 line, as demonstrated in Fig. 10. Therefore, in order to derive correct Al abundances from the Al I 3944/3961 lines, it is mandatory to take into account not only the non-LTE effect but also the background Balmer line opacities.

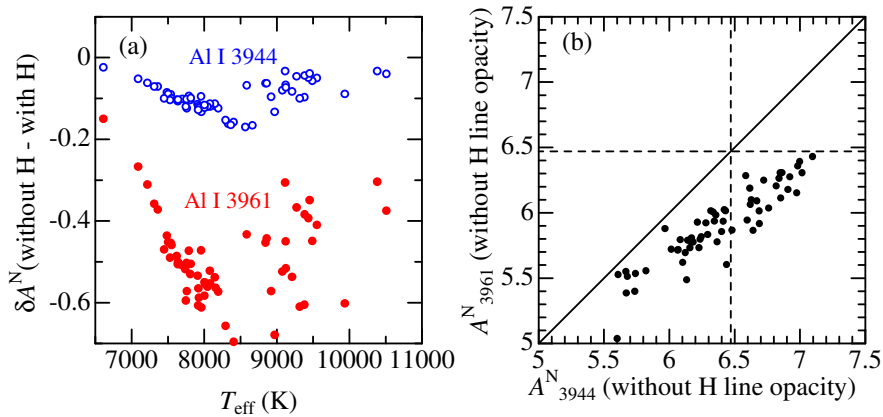


Figure 10. (a) The values of δA^N (abundance difference of two A^N values obtained by neglecting and correctly including the overlapping opacity of Balmer line wings) are plotted against T_{eff} . Open and filled symbols correspond to Al I 3944 and 3961 lines, respectively. (b) Correlation plots between A^N_{3944} (without H line) and A^N_{3961} (without H line), which should be compared with Fig. 9d (results derived by correctly including the H line opacity).

4. Other aluminium lines as abundance indicators

Finally, some discussion may be in order regarding whether and how other lines (than Al I 3944/3961 doublet) are applicable to determining Al abundances of A-type stars. Here, three candidate lines were examined: Al I 6696/6698, Al II 3900, and Al II 4663. It turned out, however, that abundances could be derived for only a limited number ($\lesssim 10$ for each line) of sharp-line stars ($v_e \sin i$ less than several tens km s^{-1}) because these lines are generally weak.

Accordingly, abundance determinations (such as done in Sect. 3.3) were carried out for 8 mostly late A-type stars (Al I 6696/6698), 6 early A-type stars (Al II 3900), and 10 early A-type stars (Al II 4663). The adopted line data are given in Table 1, and the details of spectrum fittings are presented in Table 4. The results (W , A^N , A^L , Δ) are summarized in “tableE2.dat” (6696),⁵ “tableE3.dat” (3900), and “tableE4.dat” (4663) of the supplementary materials. The accomplished fit for each region and the correlations of the resulting non-LTE Al abundances (A_{6696}^N , A_{3900}^N , and A_{4663}^N) with $\langle A^N \rangle_{3944+3961}$ are displayed in Fig. 11.

Regarding the high-excitation Al I 6696 line, which was also used by Burkhart and Coupry (1989, 1991, 2000) for their study of lower T_{eff} ($\lesssim 8000$ K) stars, A_{6696}^N is more or less consistent with $\langle A^N \rangle_{3944+3961}$ (Fig. 11b), if unreliable (yellow-crossed) data and that of HD 047105 (the very weak-line case with W_{6696} of only 1.2 mÅ) are excluded. It should be noted that positive non-LTE corrections of $\Delta \sim 0.1$ –0.3 dex are expected for this line, though comparatively less significant than in the case of Al I 3944/3961.

Rather disappointingly, the Al II 3900.675 line was found to be badly blended with the neighboring much stronger Ti II 3900.539 line, as shown in Fig. 11c. While Al abundances could be somehow determined in this synthetic fitting analysis by making use of the slight asymmetry in the blended feature, the resulting A_{3900}^N turned out to be systematically lower than $\langle A^N \rangle_{3944+3961}$ (Fig. 11d); the reason for this discrepancy is not clear. In any event, this Al II 3900 line is not suitable for abundance determination, despite that it is unaffected by any non-LTE effect ($|\Delta| \lesssim 0.01$ dex, its sign is positive or negative).

In contrast, the other Al II line at 4663 Å is much more favorable, which is almost free from any blending (Fig. 11e). Actually, A_{4663}^N and $\langle A^N \rangle_{3944+3961}$ are in satisfactory agreement with each other (though one exception is HD 060179) as seen in Fig. 11f. Since the non-LTE correction is negligibly small ($\Delta \lesssim 0.02$ dex; Δ is positive), it may be analyzed with the assumption of LTE. This Al II 4663 line would serve as a good Al abundance indicator for early A- through late B-type stars, as long as it is measurable.

5. Summary and conclusion

Although various abundance anomalies are known to be observed in the surface of A-type stars on the upper main sequence (e.g., Am stars), the behavior of aluminium abundances is still poorly understood, for which even the qualitative trend (excess or deficiency in Am stars) is not established.

That is, according to the past work on Al abundances of A stars, for which the strong resonance Al I 3944/3961 lines were mostly employed, $[\text{Al}/\text{H}]$ tends to be considerably negative for stars of near-normal metallicity ($[\text{Fe}/\text{H}] \sim 0$),

⁵Although the fitting was done in the wavelength region including both 6696 and 6698 lines, only the results for the 6696 line (twice as strong as the 6698 line) are presented here.

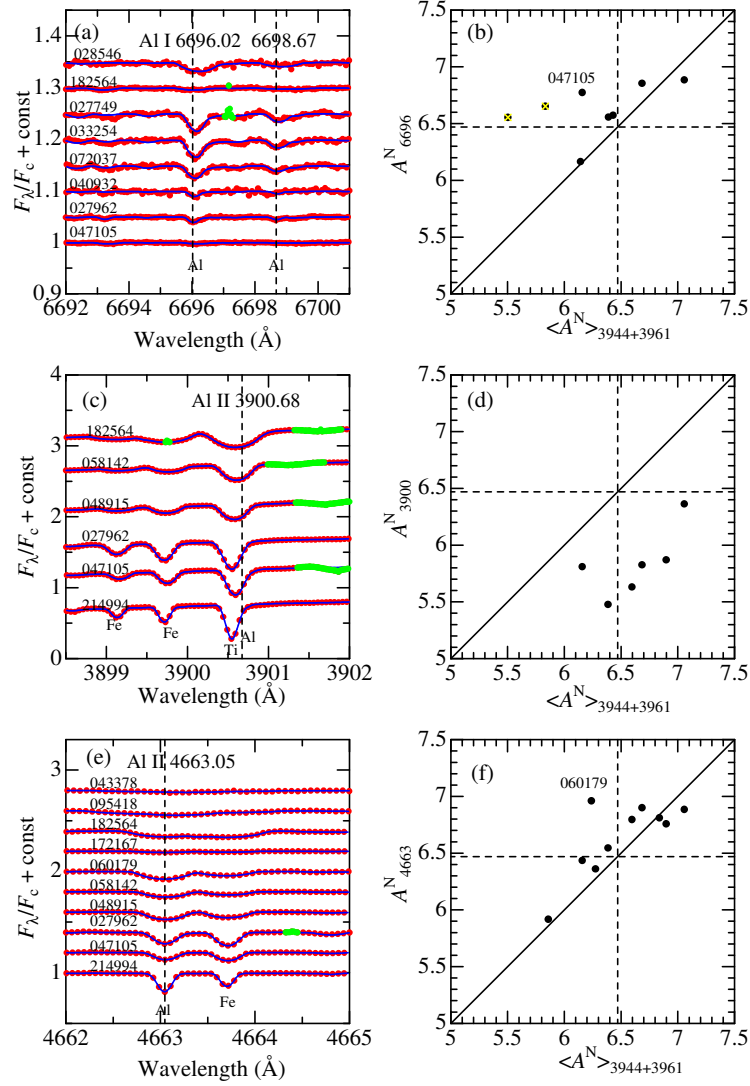


Figure 11. The left-hand panels (a, c, e) show the accomplished fit of synthetic spectrum analysis carried out for determining the abundances of Al by using (a) Al I 6696/6698 (6692–6701 Å region) (c) Al II 3900 (3898.5–3902 Å region), and (e) Al II 4663 (4662–4665 Å region). The wavelength positions of the relevant Al lines are shown by vertical dashed lines. Otherwise, the meanings of the lines and symbols are the same as in Fig. 7. The non-LTE Al abundances (A^N) resulting from these three regions are plotted against $\langle A^N \rangle_{3944+3961}$ (mean NLTE abundances of those derived from Al I 3944/3961 lines) in the corresponding right-hand panels (b, d, f), respectively. Yellow crosses are overlotted on the results based on unreliable observational data as in Fig. 9.

despite that $A(\text{Al})$ appears to be positively correlated with $A(\text{Fe})$. Moreover, the reported Al abundances derived from 3944 and 3961 lines were not consistent with each other.

This is presumably related to the fact that these previous Al abundance determinations were done with the assumption of LTE, despite that considerable non-LTE corrections are suspected for these Al I lines. Unfortunately, however, the impact of the non-LTE effect on Al abundance determination of A-type stars in general has barely been investigated so far.

With an aim to shed light on this issue, extensive statistical-equilibrium calculations on Al I/Al II were carried out for a wide range of atmospheric parameters covering early F- to late B-type main-sequence stars (6500–14000 K in T_{eff} , 3.0–4.5 in $\log g$, and -1.0 to $+0.5$ in $[\text{Fe}/\text{H}]$), and the equivalent widths (W) and non-LTE abundance corrections (Δ) for these 3944 and 3961 lines were then calculated for these model grids, which are presented as supplementary materials.

These calculations revealed that these Al I resonance doublet lines are considerably weakened by the non-LTE effect due to the overionization mechanism, which means that Δ values are always positive and significantly large ($0.3 \lesssim \Delta \lesssim 1.0$ dex) and tending to increase with W (or with a decrease in T_{eff}), where an inequality relation of $\Delta_{3944} < \Delta_{3961}$ generally holds.

As a practical application of these results, non-LTE Al abundances were determined by applying the spectrum-fitting technique to the Al I 3944/3961 lines for selected 63 A-type dwarfs ($7000 \lesssim T_{\text{eff}} \lesssim 10000$ K) of comparatively lower rotational velocities ($v_e \sin i \lesssim 100 \text{ km s}^{-1}$) based on the high-dispersion spectra obtained at the Okayama Astrophysical Observatory and the Bohyunsan Optical Astronomy Observatory.

It then turned out that consistent non-LTE abundances for both lines could be obtained and resulted in $[\text{Al}/\text{H}] \sim [\text{Fe}/\text{H}] \sim 0$ for normal metallicity stars, which means that the serious zero-point discrepancy found in old studies has been settled. This clearly indicates that applying the non-LTE corrections (and inclusion of Balmer line wings as background opacity) is indispensable for reliable Al abundance determinations of A-type stars from Al I 3944/3961 lines.

The resulting Al abundances of A-type stars are almost in proportion to $[\text{Fe}/\text{H}]$ (tending to be overabundant in Am stars) with an approximate scaling relation of $[\text{Al}/\text{H}] \sim 1.2 [\text{Fe}/\text{H}]$. This consequence is qualitatively consistent with the prediction of the diffusion theory (suggesting an Al excess in the photosphere of Am stars).⁶

As a by-product of this study, the applicability of other Al lines (Al I 6696/6698, Al II 3900, and Al II 4663) for Al abundance determination of A-type stars was also investigated. The Al II 3900 line turned out to be un-

⁶It should be remarked, however, that the situation is different for HgMn stars (chemically peculiar stars in the regime of late B-type stars), for which Al tends to be deficient as separately described in Appendix A for the case of the AR Aur system.

suitable because it is badly blended with the strong Ti II 3900 line. Yet, the Al I 6696/6698 lines (for late A-type stars; with a mild non-LTE correction of 0.1–0.3 dex) and Al II 4663 line (for early A-type stars; almost free from the non-LTE effect) may be usable as Al abundance indicators, though limited to only sharp-lined stars because of their weakness.

Acknowledgements. This investigation has made use of the SIMBAD database, operated by CDS, Strasbourg, France, and the VALD database operated at Uppsala University, the Institute of Astronomy RAS in Moscow, and the University of Vienna.

Online supplementary materials

The following electronic tables associated with this article are available at <https://www.astro.sk/caosp/Eedition/FullTexts/vol153no2/pp31-60.dat/>.

References

- Adelman S. J., 1984, MNRAS, 206, 637 [DOI: 10.1093/mnras/206.3.637]
Adelman S. J., 1988, MNRAS, 230, 671 [DOI: 10.1093/mnras/230.4.671]
Adelman S. J., 1994, MNRAS, 271, 355 [DOI: 10.1093/mnras/271.2.355]
Adelman S. J., Caliskan H., Kocer D., Bolcal C., 1997, MNRAS, 288, 470 [DOI: 10.1093/mnras/288.2.470]
Adelman S. J., Young J. M., Baldwin H. E., 1984, MNRAS, 206, 649 [DOI: 10.1093/mnras/206.3.649]
Anders E., Grevesse N., 1989, Geochim. Cosmochim. Acta, 53, 197 [DOI: 10.1016/0016-7037(89)90286-X]
Andrievsky S. M., Spite M., Korotin S. A., Spite F., Bonifacio P., Cayrel R., Hill V., François P., 2008, A&A, 481, 481 [DOI: 10.1051/0004-6361:20078837]
Arenou F., Grenon M., Gómez A., 1992, A&A, 258, 104
Asplund M., Grevesse N., Sauval A. J., Scott P., 2009, ARA&A, 47, 481 [DOI: 10.1146/annurev.astro.46.060407.145222]
Baumüller D., Gehren T., 1996, A&A, 307, 961
Baumüller D., Gehren T., 1997, A&A, 325, 1088
Burkhart C., Coupry M. F., 1989, A&A, 220, 197
Burkhart C., Coupry M. F., 1991, A&A, 249, 205
Burkhart C., Coupry M. F., 2000, A&A, 354, 216
Conti P. S., 1970, PASP, 82, 781 [DOI: 10.1086/128965]
Cunto W., Mendoza C., 1992, Rev. Mex. Astron. Astrofis., 23, 107
ESA, 1997, The Hipparcos and Tycho Catalogues, ESA SP-1200, available from NASA-ADC or CDS in a machine-readable form (file name: `hip_main.dat`)

- Ezzeddine R., Merle T., Plez B., Gebran M., Thévenin F., Van der Swaelmen M., 2018, *A&A*, 618, A141 [DOI: 10.1051/0004-6361/201630352]
- Flower P. J., 1996, *ApJ*, 469, 355 [DOI: 10.1086/177785]
- Folsom C. P., Kochukhov O., Wade G. A., Silvester J., Bagnulo S., 2010, *MNRAS*, 407, 2383 [DOI: 10.1111/j.1365-2966.2010.17057.x]
- Grevesse N., Sauval A. J., 1999, *A&A*, 347, 348
- Griem H. R., 1960, *ApJ*, 132, 883 [DOI: 10.1086/146987]
- Griem H. R., 1967, *ApJ*, 147, 1092 [DOI: 10.1086/149097]
- Hoffleit D., Jaschek C., 1991, *The Bright Star Catalogue*, 5th revised edition (New Haven, Conn.: Yale University Observatory)
- Khokhlova V. L., Zverko Yu., Zhizhnovskii I., Griffin R. E. M., 1995, *Astron. Lett.*, 21, 818
- Kurucz R. L., 1993, *Kurucz CD-ROM*, No. 13 (Harvard-Smithsonian Center for Astrophysics)
- Kurucz R. L., Bell B., 1995, *Kurucz CD-ROM*, No. 23 (Harvard-Smithsonian Center for Astrophysics)
- Lambert D. L., Warner B., 1968, *MNRAS*, 138, 181 [DOI: 10.1093/mnras/138.2.181]
- Lejeune T., Schaerer D., 2001, *A&A*, 366, 538 (DOI: 10.1051/0004-6361:20000214)
- Mashonkina L., Zhao G., Gehren T., Aoki W., Bergemann M., Noguchi K., Shi J. R., Takada-Hidai M., Zhang H. W., 2008, *A&A*, 478, 529 [DOI: 10.1051/0004-6361:20078060]
- Napiwotzki R., Schönberner D., Wenske V., 1993, *A&A*, 268, 653
- Nordlander T., Lind K., 2017, *A&A*, 607, A75 [DOI: 10.1051/0004-6361/201730427]
- Richer J., Michaud G., Turcotte S., 2000, *ApJ*, 529, 338 (DOI: 10.1086/308274)
- Ryabchikova T., Piskunov N., Kurucz R. L., Stempels H. C., Heiter U., Pakhomov Yu., Barklem P. S., 2015, *Phys. Scr.*, 90, 054005 [DOI: 10.1088/0031-8949/90/5/054005]
- Smith K. C., 1993, *A&A*, 276, 393
- Smith M. A., 1971, *A&A*, 11, 325
- Smith M. A., 1973, *ApJS*, 25, 277 [DOI: 10.1086/190270]
- Steenbock W., Holweger H., 1992, in *The Atmospheres of Early-Type Stars*, Lecture Notes in Physics, Volume 401 (Springer, Berlin), p. 57 [DOI: 10.1007/3-540-55256-1_280]
- Takeda Y., 1991, *A&A*, 242, 455
- Takeda Y., 1995, *PASJ*, 47, 287
- Takeda Y., 2020, *Stars and Galaxies*, Vol.3, id.1 (<http://www.nhao.jp/research/starsandgalaxies/03.html#2020J-1>) [DOI: 10.48550/arXiv.2012.15152]
- Takeda Y., 2022, *Contr. Astron. Obs. Skalnaté Pleso*, 52, 5 [DOI: 10.31577/caosp.2022.52.1.5]

- Takeda Y., Han I., Kang D.-I., Lee B.-C., Kim K.-M., 2008, JKAS, 41, 83
(DOI: 10.5303/JKAS.2008.41.4.083)
- Takeda Y., Han I., Kang D.-I., Lee B.-C., Kim K.-M., 2019, MNRAS, 485, 1067
[DOI: 10.1093/mnras/stz449]
- Takeda Y., Kang D.-I., Han I., Lee B.-C., Kim K.-M., 2009, PASJ, 61, 1165
(DOI: 10.1093/pasj/61.5.1165)
- Takeda Y., Kang D.-I., Han I., Lee B.-C., Kim K.-M., Kawanomoto S., Ohishi N.,
2012, PASJ, 64, 38 (DOI: 10.1093/pasj/64.2.38)
- Takeda Y., Kawanomoto S., Ohishi N., 2007, PASJ, 59, 245
(DOI: 10.1093/pasj/59.1.245)
- Takeda Y., Kawanomoto S., Ohishi N., Kang D.-I., Lee B.-C., Kim K.-M., Han I.,
2018, PASJ, 70, 91 (DOI: 10.1093/pasj/psy091)
- Talon S., Richard O., Michaud G., 2006, ApJ, 645, 634 (DOI: 10.1086/504066)
- van Leeuwen F., 2007, Hipparcos, the New Reduction of the Raw Data, Astrophysics
and Space Science Library, Vol. 350
(Berlin: Springer) (DOI: 10.1007/978-1-4020-6342-8)

A. Aluminium abundances of the AR Aur system

In the author’s previous non-LTE abundance determinations of CNO (covering up to $T_{\text{eff}} \lesssim 11000$ K; Takeda et al. 2018) and of Si (up to $T_{\text{eff}} \lesssim 14000$ K; Takeda 2022), which were based on the spectra obtained with HIDES and BOES like in this study, it was possible to derive the abundances of HgMn stars (an important group of chemically peculiar stars at $10000 \text{ K} \lesssim T_{\text{eff}}$). Unfortunately, the program stars of this investigation could contain only A-type stars of $T_{\text{eff}} \lesssim 10000$ K (and HgMn stars are lacking), because the HIDES data of late B-type stars used in the past studies do not include the short-wavelength region covering the Al I 3944/3961 lines.

However, a set of BOES spectra (of wide wavelength coverage) for AR Aur, a double-lined eclipsing binary comprising a HgMn star (primary [P], B9V) and a normal star (secondary [S], B9.5V), are available (Takeda et al. 2019). Therefore, as a supplementary analysis, non-LTE Al abundances of AR Aur (P) and AR Aur (S) were determined by applying the spectrum-fitting analysis to Al I 3944, Al I 3961, and Al II 4663 lines as done in Sect 3.3, in order to check whether any difference exists in Al abundances between normal and HgMn stars. The spectra of both stars were disentangled as described in Sect. 2.2 of Takeda et al. (2019), and the same atmospheric parameters as well as model atmospheres as used in that paper were adopted.

The results are summarized in Table 5, and the accomplished spectrum fit in each region is shown in Fig. 12, from which the following consequences can be drawn.

- As seen from Fig. 12, the Al lines are very weak and hardly detectable in AR Aur (P), which means that reliable abundance determination is not feasible. Still, $A(\text{Al}) \lesssim 5.5$ (i.e., $[\text{Al}/\text{H}] \lesssim -1$) may be concluded from Table 5 as the photospheric Al abundance for this HgMn star.
- In contrast, all three Al lines are clearly observable in AR Aur (S), and a near-solar abundance of $A(\text{Al}) \simeq 6.6$ ($[\text{Al}/\text{H}] \simeq +0.1$) is consistently obtained for this normal B9.5V star.
- In summary, while the secondary star has quite normal abundances for both Fe and Al ($[\text{Fe}/\text{H}] \simeq [\text{Al}/\text{H}] \simeq +0.1$), Al is considerably deficient in the primary HgMn star ($[\text{Al}/\text{H}] \lesssim -1$) despite that it is Fe-rich ($[\text{Fe}/\text{H}] = +0.5$).
- Two chemical abundance studies (including Al) on AR Aur based on LTE are already published. Khokhlova et al. (1995) derived $[\text{Al}/\text{H}] = -1.2$ (P) and $+0.5$ (S) from Al I 3944/3961 lines. Meanwhile, Folsom et al. (2010) concluded $[\text{Al}/\text{H}] = -1.37$ (P) and $+0.30$ (S) (though the adopted spectral lines are not explicitly described). While their results for the primary (marked Al deficiency by $\lesssim -1$ dex) are quite consistent with the consequence here, those for the secondary (moderate Al excess by several tenths dex) appear to be somewhat overestimated.
- Accordingly, unlike Am stars (for which Al-excess is accompanied with an overabundance of Fe), photospheric Al abundances in HgMn stars can be considerably deficient even for the case of supersolar Fe. This means that these two groups of chemically peculiar stars are markedly different as long as the behavior of Al abundance is concerned.
- This observational fact is a reconfirmation of the results of Smith (1993), who concluded from the analysis of UV lines based on IUE spectra that Al is deficient (becoming increasingly underabundant at higher T_{eff}) in essentially all HgMn stars.

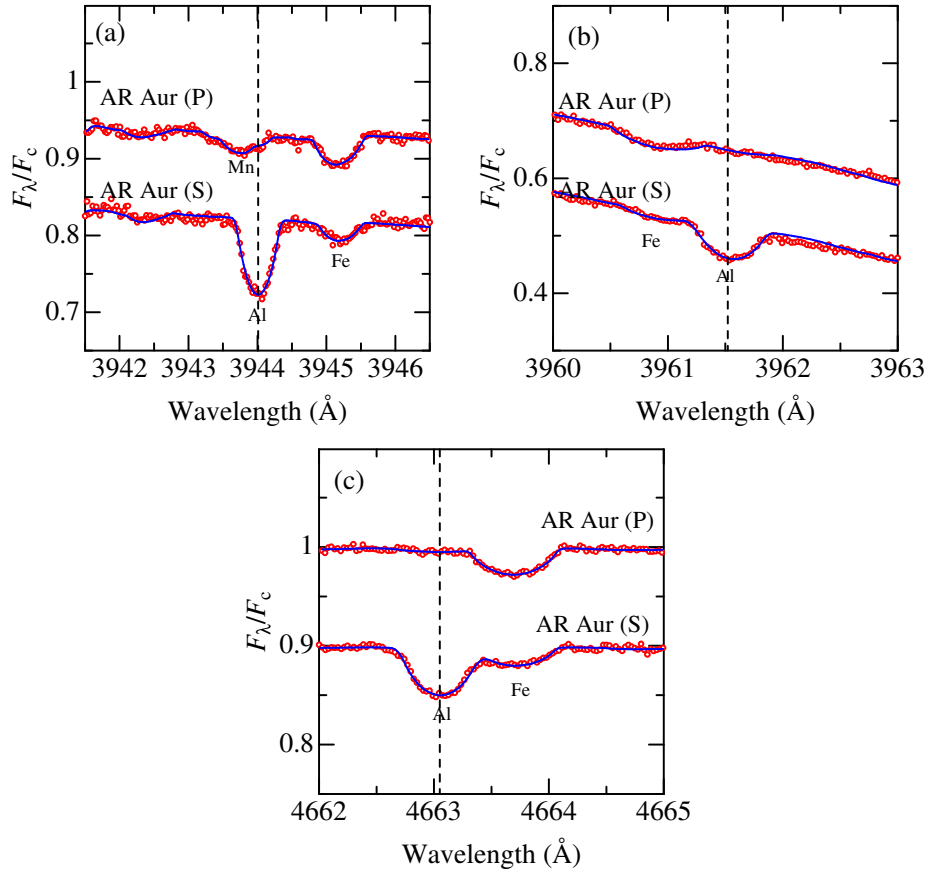


Figure 12. Synthetic spectrum fitting analysis for Al abundance determinations of AR Aur (P) and AR Aur (S) based on (a) Al I 3944, (b) Al I 3961, and (c) Al II 4663. The wavelength positions of the relevant Al lines are shown by vertical dashed lines. The scale of F_λ/F_c indicated in the left axis is for AR Aur (P), while the spectrum for AR Aur (S) is shifted downward by 0.1. Otherwise, the same as in Fig. 7.

Table 5. Analysis results of AR Aur primary (P) and secondary (S).

		AR Aur (P)	AR Aur (S)
T_{eff}	(K)	10950	10350
$\log g$	(dex)	4.33	4.28
ξ	(km s ⁻¹)	1.0	1.6
[Fe/H]	(dex)	+0.47	+0.07
W_{3944}^{N}	(mÅ)	(0.6)	48.1
A_{3944}^{N}	(dex)	(4.62)	6.55
Δ_{3944}	(dex)	+0.23	+0.30
W_{3961}^{N}	(mÅ)	(4.0)	42.8
A_{3961}^{N}	(dex)	(5.49)	6.58
Δ_{3961}	(dex)	+0.33	+0.42
W_{4663}^{N}	(mÅ)	(1.5)	24.7
A_{4663}^{N}	(dex)	(5.05)	6.66
Δ_{4663}	(dex)	+0.02	+0.03

The parenthesized data derived for AR Aur (P) are subject to large uncertainties (because the line is considerably weak and barely detectable) and thus unreliable.